Ten Years of Boundary-Layer and Wind-Power Meteorology at Høvsøre, Denmark

Pena Diaz, Alfredo; Floors, Rogier Ralph; Sathe, Ameya; Gryning, Sven-Erik; Wagner, Rozenn; Courtney, Michael; Larsén, Xiaoli Guo; Hahmann, Andrea N.; Hasager, Charlotte Bay

Published in:
Boundary-Layer Meteorology

Link to article, DOI:
10.1007/s10546-015-0079-8

Publication date:
2016

Document Version
Publisher's PDF, also known as Version of record

Boundary-Layer Meteorol
DOI 10.1007/s10546-015-0079-8

ARTICLE

Ten Years of Boundary-Layer and Wind-Power Meteorology at Høvsøre, Denmark

Alfredo Peña[1] · Rogier Floors[1] · Ameya Sathe[1] · Sven-Erik Gryning[1] · Rozenn Wagner[1] · Michael S. Courtney[1] · Xiaoli. G. Larsén[1] · Andrea N. Hahmann[1] · Charlotte B. Hasager[1]

Received: 8 July 2014 / Accepted: 27 August 2015

Abstract Operational since 2004, the National Centre for Wind Turbines at Høvsøre, Denmark has become a reference research site for wind-power meteorology. In this study, we review the site, its instrumentation, observations, and main research programs. The programs comprise activities on, inter alia, remote sensing, where measurements from lidars have been compared extensively with those from traditional instrumentation on masts. In addition, with regard to wind-power meteorology, wind-resource methodologies for wind climate extrapolation have been evaluated and improved. Further, special attention has been given to research on boundary-layer flow, where parametrizations of the length scale and wind profile have been developed and evaluated. Atmospheric turbulence studies are continuously conducted at Høvsøre, where spectral tensor models have been evaluated and extended to account for atmospheric stability, and experiments using microscale and mesoscale numerical modelling.

Keywords Atmospheric boundary layer · Remote sensing · Surface layer · Turbulence · Wind measurements · Wind-power meteorology

1 Introduction

Wind-power meteorology, related to the siting of wind turbines, estimating wind resources, and predicting wind power, has rapidly evolved with large-scale penetration of wind energy into the electricity market over the last 30 years. At present, the wind-energy fraction of the European Union's electricity consumption is 8 % and is expected to more than triple by 2030 (TPWind 2014). Such a goal, in combination with the present financial situation in

Electronic supplementary material The online version of this article (doi:10.1007/s10546-015-0079-8) contains supplementary material, which is available to authorized users.

✉ Alfredo Peña
aldi@dtu.dk

[1] DTU Wind Energy, Risø Campus, Technical University of Denmark, Frederiksborgvej 399, 4000 Roskilde, Denmark

Europe, has imposed continuous pressure on wind-turbine manufacturers, research institutes and wind consultancy agencies to find ways to reduce wind energy cost.

One way to reduce such costs is by optimizing wind turbines, i.e. to develop and design wind turbines that are optimal for the given site conditions. Test sites, where modern turbines (i.e. machines with hub heights of ≈80 m or higher) can be deployed, are required for this. More than ten years ago, the former Risø National Laboratory, now part of the Technical University of Denmark, designed and constructed such a site at the Høvsøre region in Denmark (see Fig. 1), a station where turbine manufacturers are able to test prototypes and develop commercial machines. Since then, manufacturers have rented turbine stands at Høvsøre; however, because of confidentiality and financial and legal issues, these turbine data are unavailable.

Because of Risø's interests in applied meteorology (see e.g. Petersen et al. 1998 and references therein), a mast was deployed and instrumented at eight levels. Both the site surroundings and wind conditions have drawn the attention of workers particularly in the field of wind-power meteorology. This study focuses on the research performed using ten years of measurements from instrumentation deployed on and around this mast. Our purpose is to demonstrate to both the wind-power and boundary-layer communities the spectrum of research possibilities using this database of measurements ranging from climate to turbulence studies. The study deals with technical aspects such as the sensitivity of wind-turbine power performance measurements on vertical wind shear and site selection of wind turbines. In addition, physical aspects, such as the limiting values of the wind profile and turbulence length scales beyond the surface layer, the role of baroclinity on the wind profile and turning of the wind are addressed. Furthermore, a number of studies have been undertaken to extend the usability of the industry's standard spectral tensor model under different stability conditions as well as understanding the estimation of turbulence using lidar measurements.

Section 2 introduces the Høvsøre facility (its infrastructure, masts and data management), including a review of remote sensing campaigns conducted at the site. Section 3 provides details of the roughness properties of the site from the view of the meteorological mast; most of the studies used surface-layer theory for such a characterization. In Sect. 4 we summarize the general wind climatology of the site and specific characteristics related to wind-power meteorology and wind siting; a large portion of the studies focus on improving estimates of annual energy production, as a basis for implementing wind projects. Section 5 describes a number of investigations conducted to improve the measurement of the power performance of turbines. Most of the contributions to boundary-layer meteorology are given in Sect. 6. We start by evaluating surface-layer relations at the site and the extension of such relations to the entire boundary layer. We continue by reviewing the atmospheric turbulence studies (using both the traditional and remote sensing instruments), numerical modelling and Høvsøre's usage in offshore studies. The last section provides some reflections and possibilities for future studies.

2 The Høvsøre Facility

This section introduces readers to the measurement infrastructure in place at Høvsøre. We review the history and site characteristics of the facility, including the instrumentation on the masts and remote sensing activities.

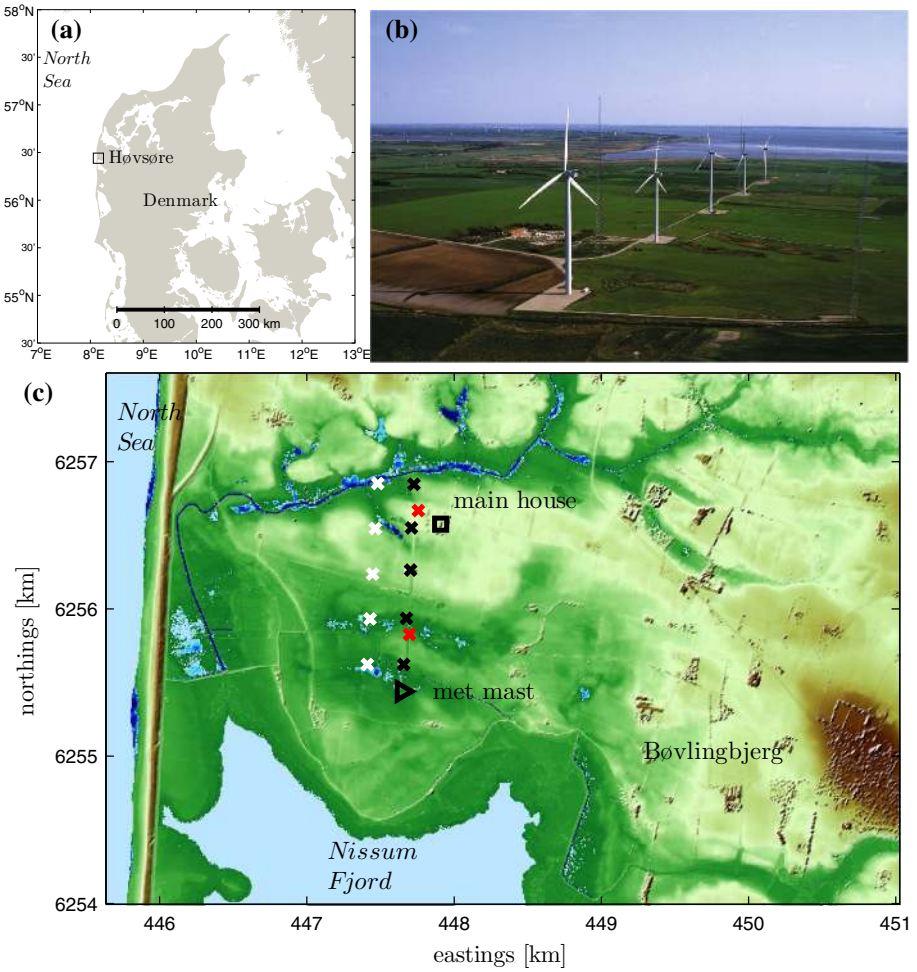

Fig. 1 **a** The Høvsøre area in Denmark. **b** A photograph (from the ≈330° direction) of the National Test Station for Wind Turbines at Høvsøre. **c** Digital surface model of the Høvsøre area (UTM WGS84) showing the locations of, among others, the turbine stands (*black crosses*), power curve masts (*white crosses*), lighting towers (*red crosses*), and the service building/main house (*black square*). *Green areas* are a mix of low vegetation areas (cropland and grassland), *light brown* a mix of cropland and artificial land, and *brown* rural areas, buildings and sand embankment. The position of the meteorological mast (*black triangle*) is 56°26′25.80″N, 8°9′2.88″E

2.1 A Short History of the Høvsøre Site Selection

The history of the National Test Station for Wind Turbines at Høvsøre, Denmark began in 1979 when a test station at the Risø National Laboratory was first established. At Risø (35 km west of Copenhagen) mean wind speeds above 20 m s^{-1} at a height of 75 m were observed only for ≈32 h each year, a value much lower than that recommended by the International Electrotechnical Commission (IEC) standards for power performance measurements (IEC 2005b) i.e. 100 h each year. This, among other constraints at the Risø site such as orographic and roughness effects, noise and operating size limitations, led the investigation of other sites for the establishment of a new test station in 1995. At that time, the hub heights of the

largest turbines were ≈50 m. However, it was already clear that the construction of even larger turbines was imminent and a site with turbines operating up to a 165-m tip height was needed. The study was conducted by the Danish Ministry of Environment and Energy together with Risø National Laboratory. It involved 20 different locations around Denmark and covered a number of topics such as meteorological and topographical conditions and noise and environmental impacts (DMEE 2000).

In 1999, the Ministry embarked on a series of public hearings after which several sites were discarded for either political reasons or noise limitations. Høvsøre turned out to be a good compromise between wind, topographical and environmental conditions (see Fig. 1, and Sects. 3 and 4 for more details); for ≈111 h each year wind speeds are >20 m s^{-1} at 80 m. Operation of the wind turbines started in 2002, and a meteorological mast deployed in February 2004 has been kept running for more than ten years.

2.2 The Høvsøre Site

Høvsøre is a nearly flat (max. height variations of 5 m in an ≈7-km radius) coastal farmland area in west Jutland, Denmark. It has no major obstacles other than the village of Bøvlingbjerg and a coastal sand embankment with a width of ≈40–50 m and ≈12-m height separating the North Sea from the grasslands (see Fig. 1).

The test station is located at ≈3 km north-west of Bøvlingbjerg and 1.7 km east of the North Sea at an average height of 2 m above mean sea level. The Nissum Fjord lies ≈800 m south of the station's (116.5 m) meteorological mast. The site also comprises five turbine stands (which turbine manufacturers rent for machine testing and research, each with a 'power curve' mast), two lighting towers and a central service building (see Fig. 1c). The University does not own any of the machines at the station; therefore, we focus here on the mast measurements rather than the turbines.

2.3 The Høvsøre Masts

Three types of mast towers are installed at the station: the meteorological mast south of the station, five 'power curve' masts north to south along the station, and two lighting towers in between the turbines.

2.3.1 Meteorological Mast

This mast, also known as the Høvsøre mast, is equipped with meteorological equipment from below the surface up to 116.5 m; all levels hereafter refer to the ground (see Table 1; Fig. 2). The mast is an equilateral triangular lattice structure with a width of 7.15 m at the ground, decreasing to 1.10 m at 100.5 m (one vertex points to the east with one of the bases aligned in a north-south direction). The instruments are installed on booms protruding from the mast at 6.0, 4.3 and 1.9 m at heights of 59.7, 80.5, and 100.5 m, respectively; cup anemometers and vanes are installed on the south boom and sonic anemometers on the north booms. The 116.5-m cup anemometer is top-mounted on a 2-m pole. The theoretical wind-speed deficits, estimated as the ratio of the wind speed that an instrument measures at its position on the mast (taking into account the physical and geometric characteristics of the mast, booms and clamps) to that which the anemometer should measure in a 'non-distorted' installation, are ≈1.5, 1.1 %, and zero for the 40- and 100-m, 60- and 80-m, and the pole levels, respectively. This was estimated for the direction 270° from the IEC power performance guidelines (Eq. G.1 in IEC 2005b).

Table 1 Instrumentation on the meteorological mast at Høvsøre, Denmark

Measurement	Instrument	Height (m)
Wind speed	Risø P2546A cup anemometer	2, 10, 40, 60, 80, 100, and 116.5
Wind direction	Risø P2021A wind vane	10, 60, and 100
Relative	F2920A Vaisala HMP45A RH/	2 and 100
Humidity	T probe radiation shield	
Temperature	Risø P2642A sensor	2, 40, 60, 80, and 100
Gradient	Risø P2029 radiation shield	(relative to the lowest level–2)
Temperature	Risø P2449A sensor/	−0.05, 2, and 100
(Absolute)	Risø P2029 radiation shield	
Pressure	P2717A Vaisala barometer PTB100	2 and 100
Turbulence	Metek USA1 F2901A sonic	10, 20, 40, 60, 80, and 100
Solar radiation	F2253C CM11 pyranometer	2

The effect on the cup and sonic anemometer measurements of the mast/boom structure is illustrated in Fig. 3, where the wind-speed ratio between the two measurements as function of the wind direction from the vane at the same level is presented. For two different heights, the northern sector (influenced by the turbines' wakes and where the cup anemometers are directly in the wake of the mast) and the southern one (where the sonic anemometers are directly in the wake of the mast) show the greatest difference from the ideal set-up (=1), whereas the lowest differences are within the eastern and western sectors. Most studies using data from the mast and referred to herein are restricted to the westerly and easterly directions because these also correspond to the predominant and more homogenous sectors, respectively (see Sects. 3 and 4). Mast distortion effects are generally neglected in most meteorological studies at Høvsøre. However, note that we observed the wake of the mast as far as 50 m downwind using remote sensing measurements (Nikola Vasiljevic, personal communication, 2014).

2.3.2 Power-Curve Masts

These five lattice masts are located 250 m west of the turbine stands (2–2.5 rotor diameters for the turbines tested at Høvsøre) to comply with the IEC requirements for power-curve measurements (IEC 2005b). The power curve is the relation between a characteristic wind speed, normally measured at hub height, and the power extracted by the turbine. The masts are instrumented with cup anemometers, vanes, pressure, temperature and rain sensors similar to those on the meteorological mast at different levels; however, these depend on the turbine size (other sensor brands are used in some of these masts following the requirements of the turbine manufacturers). More details are given in Sect. 5.

2.3.3 Lighting Towers

There are two obstructing 160-m lighting towers within the row of turbines. The southern tower is equipped with sonic and cup anemometers, vanes, including temperature measurements at 100 and 160 m, and are of the same type as those on the meteorological mast. These

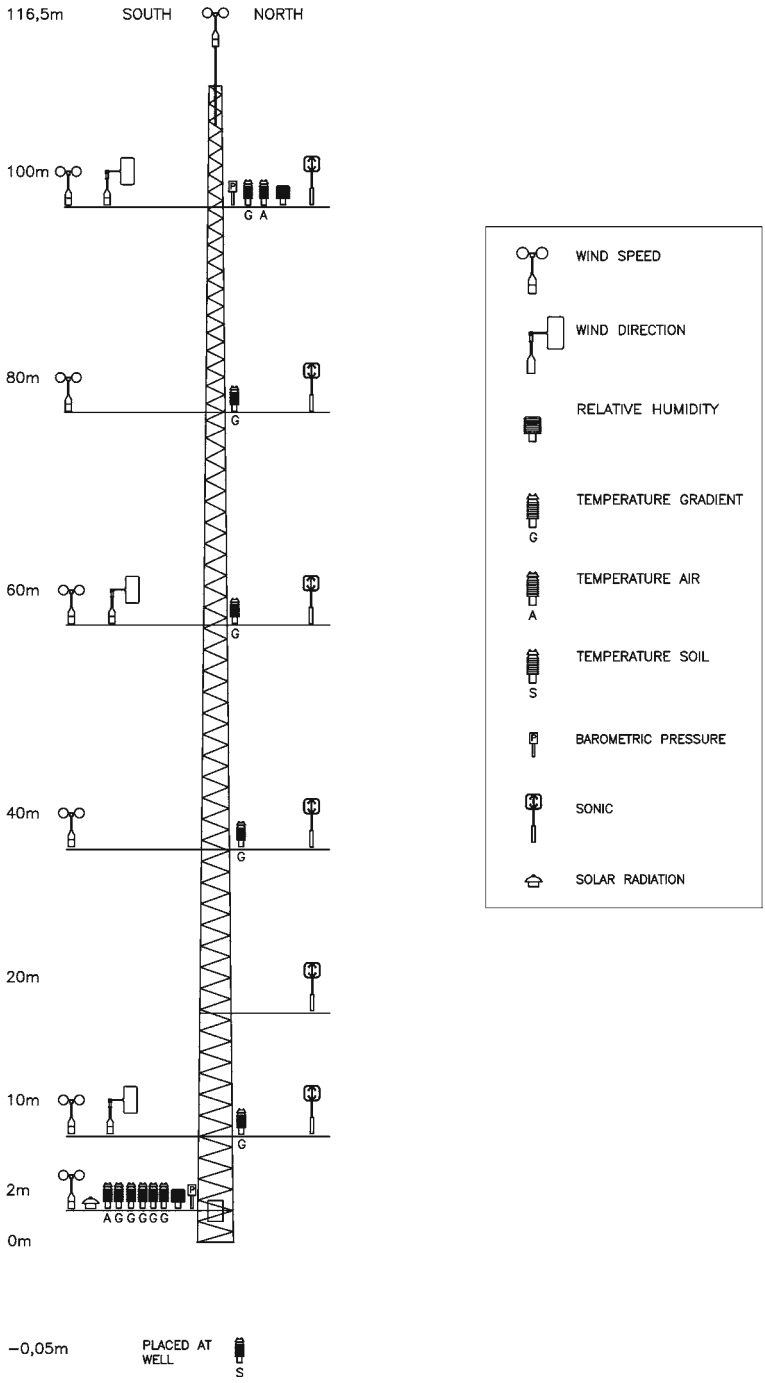

Fig. 2 Sketch of the Høvsøre meteorological mast and its instrumentation

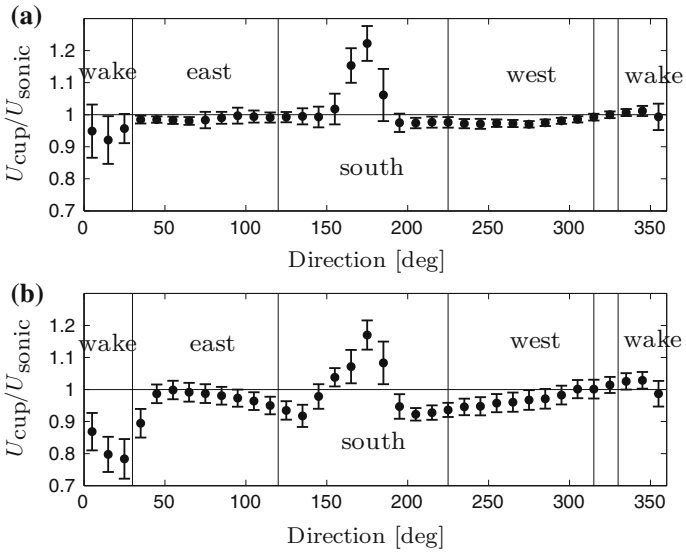

Fig. 3 Ratio between cup and sonic anemometer wind speed (U) as a function of the wind direction from the vane at two different levels at **a** 100 m and **b** 10 m at the Høvsøre meteorological mast based on 10-min mean observations for the period 2005–2013. The *markers* represent the mean and the *error bars* ±one standard deviation. *Vertical lines* show the boundaries of the different wind sectors

measurements can be used to vertically 'extend' those at the meteorological mast under easterly flow conditions because the observations are not affected by the wakes of the turbines (Gryning et al. 2007; Peña et al. 2010a).

2.4 Remote Sensing

The meteorological mast is used for calibrating ground-based lidars and sodars (Bradley et al. 2005), with the lidar to be calibrated placed close to the mast on a stable platform. The Technical University of Denmark has an established procedure for the calibration of lidars, accredited by the Danish Accreditation and Metrology Fund. The lidar wind-speed measurements are compared to those from the cup anemometers at the mast and the measurement uncertainty of the lidar at each height is determined (Hasager et al. 2013). The sensitivity of the lidar wind-speed measurement to e.g. vertical wind shear and turbulence intensity, are also studied (Albers et al. 2012). Secondary variables, such as the direction measurement, are also tested by comparison to the vanes, as well as the lidar-sensing height error (Lindelöw-Marsden 2007). A lidar was also placed at Høvsøre to determine its accuracy when estimating flow tilt angles (Dellwik et al. 2010).

Ground-based lidars provide accurate measurements of 10-min winds, but turbulence measurements from lidars are different from those of sonic or cup anemometers (see Sect. 6.3.2 for details). The feasibility of performing three-dimensional turbulence measurements with lidars was demonstrated by Mann et al. (2009), who crossed the beams of three pulsed lidars close to a sonic anemometer at 78 m and found attenuation of the variance of the lidar velocity due to spatial filtering.

Nacelle-mounted lidars have been considered for wind-turbine power performance verification (see Sect. 5 for details). A method was developed for the calibration of two-beam

nacelle lidars at Høvsøre and the various uncertainty sources in the lidar wind-speed measurement were determined by Wagner et al. (2013). The horizontal wind-speed measurement uncertainty is ≈1–3 % for the range between cut-in and rated turbine wind speeds. This type of lidar has not yet been accepted by the standards' authorities (IEC 2005b) as a possible replacement for masts.

The accuracy of the scanning lidars has also been tested with a WindCube®200S lidar, which was installed at 1.6 km from the meteorological mast and configured to perform sector-scanning around the top cup anemometer at 116.5 m. The reconstructed lidar horizontal wind speed on average overestimated that of the cup by 0.8 % (Courtney et al. 2014). The measurement uncertainty was sensitive to the wind direction, being higher at wind directions orthogonal to the laser beam.

2.5 Data Management

Detailed information on the management of the Høvsøre data can be found at http://www.vindenergi.dtu.dk/Om_instituttet_tekst/Hoevsoere/Data-Management. At this weblink there is a description of the data infrastructure and data processing, starting with the acquisition of observations and quality control strategies up to the procedure to access the Høvsøre database.

3 Roughness and Land-use Properties

Here we provide an overview of studies in which the aerodynamic roughness length at Høvsøre has been determined, as this is one of the most important parameters for flow characterization, and suggest ways to account for roughness when performing long-term analysis at Høvsøre. Long-term is here referred to at least 1 year of records performed up to a frequency of ≈1 h.

The surface characteristics at Høvsøre depend on the season and mainly on the upstream footprint area (Blatt 2010). The aerodynamic roughness length z_o has been estimated from the analysis of mean wind profiles, typically using the diabatic wind profile

$$U(z) = \frac{u_*}{\kappa}\left[\ln\left(\frac{z}{z_o}\right) - \psi_m\left(\frac{z}{L}\right)\right], \tag{1}$$

where $U(z)$ is the mean wind speed at a height z, κ is the von Kármán constant (= 0.4), and u_* is the friction velocity. ψ_m is a stability correction term that depends on the Obukhov length L,

$$L = -\frac{{u_*}^3}{\kappa(g/T)\overline{w'\Theta'_v}}, \tag{2}$$

where g is the acceleration due to gravity, T is a 'mean' reference temperature, w is the vertical component of velocity, θ_v is the virtual potential temperature, and $\overline{w'\theta'_v}$ is the virtual kinematic heat flux, where the prime denotes fluctuations around the mean value and the overbar is a time average.

Gryning et al. (2007) adjusted the value of z_o in Eq. 1 to match the 10-m average wind speed under a given atmospheric condition (the 10-min profiles were classified into a number of stability classes based on the values of L estimated from the sonic anemometer at 10 m). Thus, z_o appears to be a function of atmospheric stability; they found $z_o = 0.014$ m under neutral conditions and slightly increasing and decreasing values under unstable and stable

conditions, respectively. These values represent long-term estimates of z_o, performed over a two-year period and for easterlies only. Similarly, Peña et al. (2010c) used the logarithmic wind profile (i.e. Eq. 1 with $\psi_m = 0$) to estimate z_o and found that for both winter and a three-year period, $z_o \approx 0.016$ m under neutral conditions. Peña et al. (2010b) found nearly the same values as Gryning et al. (2007) for a range of stabilities and further classified the neutral cases into wind-speed ranges; z_o was found to decrease with wind speed.

Blatt (2010) analyzed a four-year period and used four methods to estimate z_o. The yearly median z_o for three of the methods is ≈0.010 m, whereas the fourth, which is based on the standard deviation of the horizontal wind speed, gives about half this value due to the large footprints covered by this wind component. All methods show the highest mean z_o values in July and lowest in December–January (≈0.023 and ≈0.007 m, respectively).

As an overview of the direction and seasonal roughness changes, a roughness rose is presented in Fig. 4 for the period 2005–2013. The analysis was performed over 10-min averages where $|L| > 1000$ m at the 10-m sonic level and fitting of the logarithmic wind profile to observations at different levels using the 10-m sonic-derived friction velocity was conducted. Blatt (2010) compared the results of the inter-annual variation of z_o when using either near-neutral or diabatic wind-speed observations, and found slight differences in winter (the largest in December where the near-neutral z_o is ≈0.010 m and the diabatic value ≈0.007 m).

Generally, the highest z_o values found are for northerly, south-easterly and westerly winds, which correspond to flow from the most heterogeneous directions. Choosing different levels for the logarithmic wind-profile fit does not have a strong effect on z_o except for the wake-affected sector. Autumn, winter, and spring roughness roses are very similar, the autumn one systematically showing the highest z_o values. The summer z_o values are, for most directions,

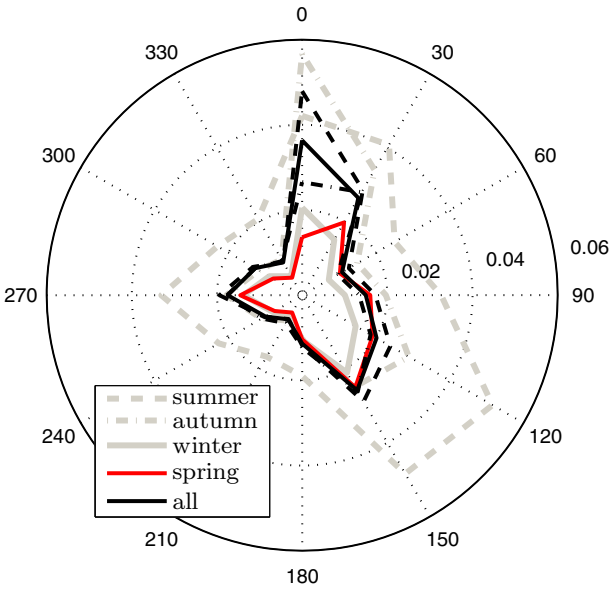

Fig. 4 Variation of the roughness length with direction and season at Høvsøre for neutral conditions only. The radii of the *circles* represent the roughness length value in m. *Solid*, *dashed*, and *dash-dotted black lines* show the roughness estimations found by fitting the logarithmic wind profile to the wind-speed observations at 40, 10, and 2 m, 40 and 10 m, and 10 and 2 m, respectively

about two times higher than those observed during winter. Peña et al. (2010a) found, under neutral conditions and within a three-month summer period, z_o values that were three times higher than those in Peña et al. (2010b), who used a much longer dataset.

The values shown in Fig. 4 are median values over 30° sectors. However, the distribution of 10-min z_o values for each sector extends in many cases for more than three orders of magnitude. Such wide z_o distributions are found under any stability, season, direction, for all analysis methods, and using any level on the mast. This is because of the errors in modelling the wind profile at Høvsøre with Eq. 1 (Peña et el. 2015b) and because one can only assume a constant z_o value per sector when performing a long-term analysis. For such an analysis, a map with a roughness description reflecting the findings illustrated with the solid black line in Fig. 4 is recommended.

4 Wind Climate at Høvsøre

Here, we review the general wind conditions and climate at Høvsøre. We also describe the specific characteristics of the site in relation to wind-power meteorology and wind siting.

4.1 Wind Conditions

At Høvsøre the observed long-term mean wind speed at 100 m is 9.3 m s^{-1} with low turbulence levels (see Sect. 4.3). Figure 5a illustrates the wind rose of 10-min wind speeds observed at the meteorological mast at 100 m over a period of nine years. North-westerly winds are predominant at the site, and most winds are thus influenced by the North Sea. Northerly winds are rare and so wakes from the turbines are not often seen at the meteorological mast. Estimations of geostrophic winds from simulations made with a mesoscale model, shown in Fig. 5 (see details of such estimations in Sect. 6.4.1), also lack the northerly winds and show a similar wind pattern.

The hourly, daily, monthly and annual variability of wind speed is shown in Fig. 5c. The intra-annual variability is high; wind speeds are higher in winter than in summer with 100-m hourly wind speeds exceeding 30 m s^{-1} on occasions. The inter-annual variability is also high; the difference in wind speed between 2006 and 2007 is ≈10 %.

Floors et al. (2011) showed that, for westerlies, the long-term diurnal behaviour of atmospheric stability observed at the 160-m sonic anemometer level on the lighting tower is similar to that at the Horns Rev offshore site (19 km west of Denmark's most western land point and ≈100 km from Høvsøre). When analyzing the stability behaviour closer to the ground, unstable conditions are mostly observed around midday, whereas stable conditions dominate the nighttime as illustrated in Fig. 6a. A clear diurnal variation is found for the stability close to the ground and at a height of 160 m for easterlies only (Fig. 6c); such a variation is damped for westerly winds at 160 m (Fig. 6b) as these partly reflect the upwind offshore conditions. Refer to Peña et al. (2012) to see the diurnal variation of the vertical wind shear, which is closely linked to stability, for a number of offshore sites compared with Høvsøre. An intra-annual variation is also observed at Høvsøre (Fig. 6d); in winter, very stable conditions are not so common, with less stable and neutral conditions the most frequent. Neutral conditions increase in percentage with increasing wind speeds (Fig. 6e); at ≈10 m s^{-1} more than 70 % of the data are near-neutral. Wind speeds are generally the highest in winter explaining the increase of near-neutral conditions during this season.

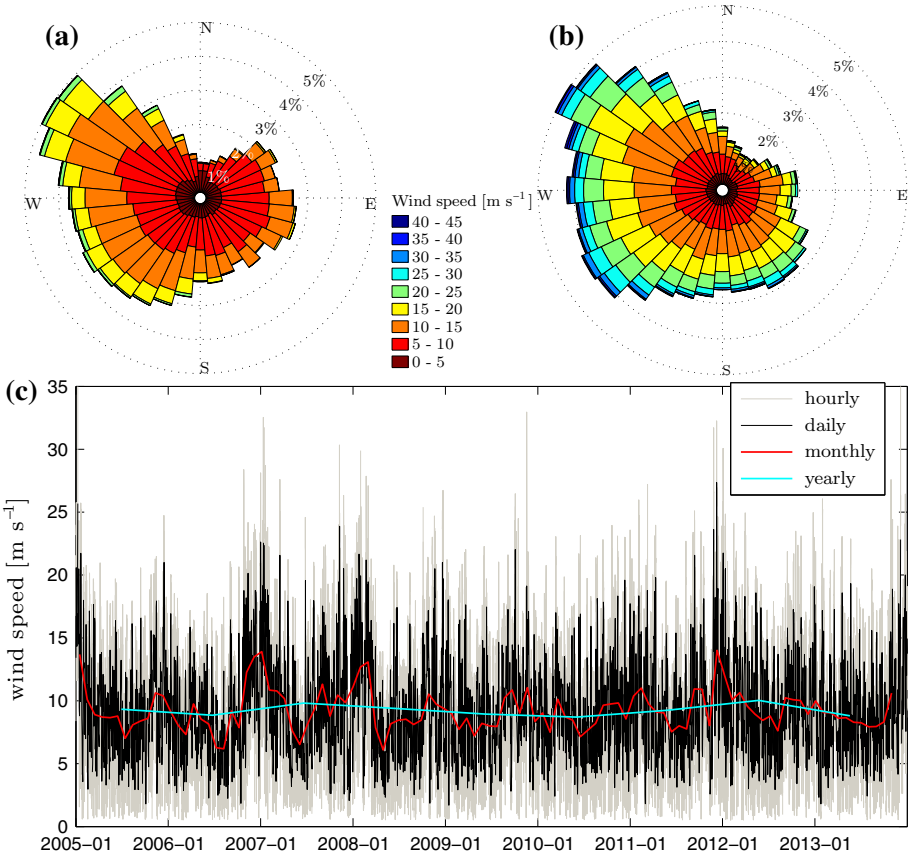

Fig. 5 **a** Wind rose of 10-min wind speeds observed at the meteorological mast at 100 m for the period 2005–2013. **b** Wind rose of simulated geostrophic winds for the period 2005–2012. **c** Time series of the 100-m mean hourly, daily, monthly, and annual wind speed for the same period

4.2 Wind-Power Meteorology

4.2.1 Wind-Power Climatology

The Weibull distribution,

$$f(x) = \frac{k}{A}\left(\frac{x}{A}\right)^{k-1} \exp\left[-(x/A)^k\right], \tag{3}$$

where $f(x)$ is the frequency of a variable x (U in our case), and A and k are the parameters representing the scale and shape of the distribution, respectively, is traditionally used to characterise mean wind-speed frequencies per sector (normally 12, numbered clockwise with sector 1 facing north). The power density ($= (1/2)\rho\overline{U^3}$, where ρ is the air density) can also be estimated from the Weibull parameters as $(1/2)\rho A^3\Gamma\,(1 + 3/k)$, where Γ is the Euler gamma function.

The all-sector mean wind-speed histograms at Høvsøre follow the Weibull shape at all levels (see Fig. 7a for the 100-m level only) for each sector. The figure illustrates that by using A and k, estimated using a maximum likelihood estimator, the Weibull-derived long-term

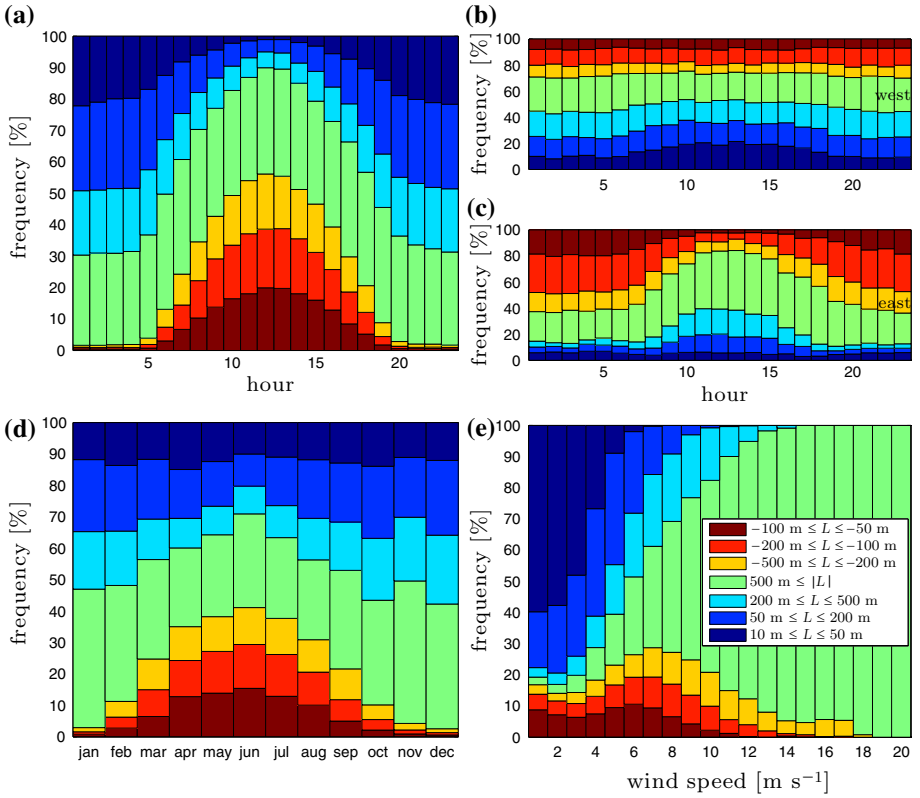

Fig. 6 Frequency of occurrence of stability classes based on the 10-m sonic on the meteorological mast. **a** per hour, **d** per month, and **e** per wind speed observed at 10 m. **b**, **c** frames are also per hour but for westerly and easterly wind conditions, respectively, based on the 160-m sonic on the southern lighting tower

mean wind speed ($\overline{U}$) and power density are close to the values derived from the time series. The inter-annual and directional variations of A and k were studied by Perez-Andujar (2013), who found maximum yearly differences of 5 and 4 % for A and k, respectively.

Figure 7b illustrates the all-sector long-term wind profile observed at the mast and estimations from the logarithmic wind profile. For the latter, $z_o = 0.012$ m is estimated by fitting Eq. 1 with $\psi_m(z/L) = 0$ to the long-term wind speed at 10 m and the long-term u_* computed from the average of 10-min u_* estimations from the sonic anemometer at 10 m. The wind profile from the microscale model included in the Wind Atlas Analysis and Application Program (WAsP) (Mortensen et al. 2007) is also shown. Here the observed wind climatology at 10 m is used in WAsP to extrapolate the wind speed up to 100 m and the result is closer to the observations than when using the logarithmic wind profile. The roughness specification was overlaid on a digital map of the orography and reflects the z_o variation shown with the black solid line in Fig. 4.

For energy estimates, we require an accurate long-term wind profile reflecting the site conditions. Kelly and Gryning (2010) developed a long-term wind profile, where the long-term stability correction is estimated from the distribution of stabilities at the site. Both the theoretical envelope of the distribution of the long-term stability and the long-term wind profile showed good agreement compared to observations from a number of masts, including that at Høvsøre.

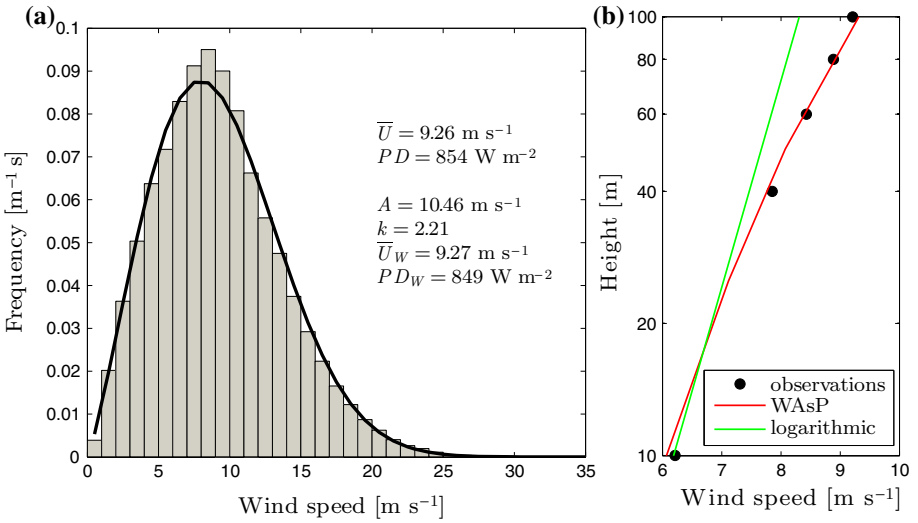

Fig. 7 **a** Histogram of 10-min mean wind speeds observed at the meteorological mast at 100 m for the period 2005–2013 (*grey bars*). The Weibull fit is shown in the *solid black line* and the A and k values are also given. The long-term mean wind speed ($\overline{U}$) and power density (PD) of both the 10-min time series and the Weibull fit (subscript $_W$) are also shown. **b** The all-sector long-term vertical mean wind profile observed at the mast (*markers*). The logarithmic wind profile (*green*) and the WAsP profile (*red*) are also shown

4.2.2 Vertical Profiles of Weibull Parameters

Based on 1-year long mast and lidar measurements at Høvsøre, profiles of the A and k parameters have been analyzed (Gryning et al. 2014). A was found to be nearly proportional to the mean wind speed; k was small near the ground, reached a maximum at a level that depends of the inflow wind conditions, and decreased upward. For easterlies, the k-maximum occurs at ≈100 m, and for westerlies, k is smaller with a maximum at ≈50 m. The k-profile parametrization in Gryning et al. (2014) agreed well with observations for both the land and coastal sectors.

Over land the k-profile's shape and the height at which k is greatest (reversal height) are controlled by the local meteorological conditions. A small value of k is observed at 10–40 m, due to the large diurnal variation of the wind speed close to the ground. At about 100 m there is little diurnal variability in the wind speed, and the behaviour is reversed upwards, the wind speed being higher during the night. Changes in the planetary boundary-layer (PBL) height between night and day might explain this behaviour. Low-level jets (LLJs) are often observed on top and above the stable boundary layer and contribute to the effect. This phenomenon is important for wind energy because energy estimations are based on the hub-height wind speed; energy production for small turbines is thus lower during the night. For very large turbines the nighttime production is higher. Kelly et al. (2014) reported similar results based on the meteorological mast measurements only.

For flow from the sea, the diurnal variability of wind speed follows almost the same pattern at all heights and the variation in the energy production is less dependent on the turbine size. The reversal height is also much lower and the maximum in k is less pronounced; the lower part of the k-profile is partly controlled by the developing internal boundary layer (IBL) and the upper part reflects the marine conditions. Floors et al. (2011) found that the stress-derived

IBL at the Høvsøre mast is about twice as high as that based on wind velocity. Recent analysis shows that the reversal height is about a third of the height of the stress-derived IBL. Thus, the velocity-based IBL can be used to estimate the reversal height.

4.3 Wind-Turbine Siting

In day-to-day wind-energy applications a turbine is selected and its safety verified by checking that the particular site conditions are less severe than those assumed during the turbine design following the IEC design standard (IEC 2005a). The basic characteristics of the Høvsøre site for turbine deployment are related to the following:

1. Wind shear. The all-sector wind profile (Fig. 7b) has a shear coefficient α of 0.16, estimated from the power law
$$U(z) = U_{\text{ref}}\,(z/z_{\text{ref}})^{\alpha}\,, \tag{4}$$
where U_{ref} and z_{ref} are the reference height and mean wind speed, respectively. We chose $z_{\text{ref}} = 80$ m and $z = 100$ m because these are the two levels with observations closer to the hub height of the Høvsøre turbines. IEC (2005a) recommends $0 < \alpha < 0.2$ to avoid blade-tower interaction and enhanced fatigue damage.
2. Extreme winds; see Sect. 4.4.
3. Turbulence intensity. Figure 8 illustrates the observed turbulence intensity (TI), computed as the ratio of the standard deviation to the mean wind speed within 10-min intervals, σ_U/U, using the 100-m cup anemometer measurements for a range of wind speeds where turbines typically operate. The analysis is performed for the west and east sectors (same as those in Fig. 3) and includes the three curves from the IEC standard, which are defined as
$$TI = TI_{\text{IEC}}\,[0.75U(z) + B]\,/\,U(z), \tag{5}$$
where TI_{IEC} is a reference TI (= 0.16, 0.14, and 0.12 for turbine classes A, B, and C, respectively) and B is a constant (= 5.6 m s^{-1}). According to the IEC standard the computed 90% percentile from the observed TI should be lower than the curve of the selected turbine (given by Eq. 5) within the range ≈8–25 m s^{-1}. As illustrated, the western sector complies with all turbine classes and the eastern sector with class A only. Due to the low turbulence levels at Høvsøre, the uncertainty of the turbines' power curves is generally low.
TI values are generally lower for the western compared to the eastern sector. The behaviour of TI with wind speed is mainly due to stability effects, which are more pronounced at the low wind-speed range. When selecting near-neutral conditions TI is nearly constant with wind speed for easterlies at Høvsøre (Peña et al. 2015a). The figure also shows in the solid grey line an estimation of TI assuming $\sigma_U = 2.5u_*$, which, combined with Eq. 1 with $\psi_m = 0$, results in the relation $TI = \ln(z/z_o)^{-1}$ (we use $z = 100$ m and $z_o = 0.012$ m as in Fig. 7b). The observed TI of the eastern sector approaches such an estimation in the high wind-speed range.

4.4 Extreme Winds

From 2004 to 2010 the 10-min measurements of wind speed and direction at multiple levels were used to validate simulated storms using the Weather Research and Forecasting (WRF) mesoscale model (Skamarock et al. 2008) (see Sect. 6.4.1 for more studies where the WRF model is used) and the omni-directional 50-year wind speed at 100 m estimated from the

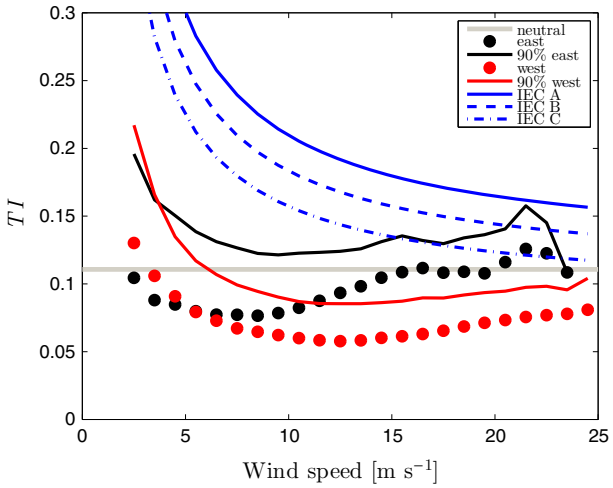

Fig. 8 Turbulence intensity (TI) as function of the wind speed. The *black* and *red markers* represent the average TI (within 1 m s^{-1} bins) for the east and west sectors, respectively, from measurements of the 100-m cup anemometer at the Høvsøre mast during 2005–2013. *Lines* with the marker's same *colours* represent the 90 % percentiles. *Blue lines* show TIs for different turbine classes based on the IEC standard and the *grey line* shows the estimation of TI for neutral conditions (see text for details)

selective dynamical downscaling method developed in Larsén et al. (2013a). The 10-min 50-year wind speed at 100 m was estimated to be 44 m s^{-1} with a 95 % confidence interval of 12.5 m s^{-1}.

Power spectra have also been calculated from the 10-min wind measurements. The measured spectral behaviour follows the general description of the spectral model for the mesoscale range (Larsén et al. 2013b). Due to smoothing effects in the numerical modelling, such as the temporal and spatial resolution of the large-scale forcing, the wind power spectrum shows a tapered-out tail in the high frequencies (Skamarock 2004), leading to underestimation of the extreme value by mesoscale models (Larsén et al. 2012). The spectral model obtained from measurements (Larsén et al. 2013b) seems to help recover this missing variability. The smoothing effect might be reduced with increasing spatial resolution. The estimates of the extreme wind speed discussed earlier are from storm simulations from the WRF model with a 5-km resolution and an underestimation of 3 % was calculated from spectral analysis (Larsén et al. 2012).

The Høvsøre observations can be used to evaluate the conventional method for estimating the gust value at high altitudes, which uses a Gaussian process and a turbulence model (Suomi et al. 2014). The gust measurements were also used to validate the non-local gust approach proposed by Brasseur (2001). Larsén and Kruger (2014) applied this approach and they used the WRF model to simulate extreme gusts during storms. The gust simulations captured the magnitude of the measured gust at heights >40 m and further development is needed to extend this approach to lower levels.

5 Wind-Turbine Power-Performance Measurement

Wind turbines with tip heights up to 160 m can be deployed at the five test pads at Høvsøre. These are rented to manufacturers to test prototype turbines.[1] Various types of turbines with

[1] http://www.vindenergi.dtu.dk/English/About/Hoevsoere_uk.aspx.

hub heights between 80 and 113 m, rotor diameters up to 130 m, and nominal power up to 6 MW were tested at Høvsøre between 2002 and 2014, including 2 Neg Micon (nowadays Vestas), 12 Vestas, 3 Bonus (nowadays Siemens), 7 Siemens, and 4 Nordex machines.

The Høvsøre site has been useful for investigating power-performance measurement techniques. First, the effect of vertical wind shear on wind-turbine power curves was demonstrated based on aeroelastic simulations and mast measurements (Wagner et al. 2009) and turbine and lidar measurements (Wagner et al. 2011). The site experiences a range of wind-speed profiles for different directions, due to large thermal effects for easterly winds and the influence of the abrupt change of roughness for westerlies. Wind profiles deviating from the diabatic wind profile (see details in Sect. 6.1) are observed mainly from the western sector in spring and autumn when the difference between the land and sea temperatures is relatively large. A wind speed representative of the whole profile, a weighted-average wind speed over the swept rotor area, was found to significantly reduce the sensitivity of the power curve to vertical wind shear (Wagner et al. 2011). This was accomplished using a ground-based lidar.

A 'nacelle lidar for power curve measurement' campaign took place at Høvsøre (Wagner et al. 2014) from September to November 2010. This was conducted with a two-beam nacelle lidar prototype, which can also be used for offshore turbines as the flow over water can be assumed to be horizontally homogeneous (under wake-free sectors). Although the IBL significantly influences the westerly flow at Høvsøre (see Sect 6.2.2), the characteristics of such a flow are close to those of an offshore site (see e.g. Fig. 8) with advantages in accessing the turbine and instrumentation.

6 Atmospheric Research at Høvsøre

Here we illustrate research activities related to the measurement and modelling of the atmosphere at Høvsøre. Evaluation of the Monin-Obukhov similarity theory (MOST) (Obukhov 1971), extension of wind-profile parametrizations beyond the surface layer, IBL analysis, investigation of the turbulence structure and evaluation of numerical models, are also presented.

6.1 Surface Layer

In the surface layer, MOST has been used to describe the turbulent flow at Høvsøre. MOST states that assuming stationarity and flow homogeneity, dimensionless groups of mean vertical gradients are functions of the stability parameter z/L. The dimensionless wind shear can then be expressed as $\phi_m = (l/u_*)\,\partial U/\partial z$, where l is the length scale of the surface layer ($l = \kappa z$), from which the diabatic wind profile, Eq. 1, can be derived. Equation 1 has been used to model the surface-layer wind profile at Høvsøre. Gryning et al. (2007) found that for a two-year period, easterly surface winds agreed well with the observations using the ψ_m expressions of Dyer (1974). Similarly, Peña (2009) and Sathe et al. (2013) found that commonly used expressions for ψ_m suited the easterly surface wind profile for a range of stability classes based on four years of data. These works show that the diabatic wind profile is accurate in describing the vertical wind shear up to a height that depends on the stability of the surface layer, for very unstable and stable conditions up to 160 and 40 m, respectively.

Using the polynomial form of Högström (1988), ϕ_m can be computed from wind-speed measurements combined with sonic observations of u_*. Figure 9 illustrates ϕ_m as a function of stability (derived from the sonic anemometer at 10 m) where $u_* > 0.1$ m s^{-1}. Here, we compare the observations of ϕ_m with the extensive re-evaluation of the Businger-Dyer

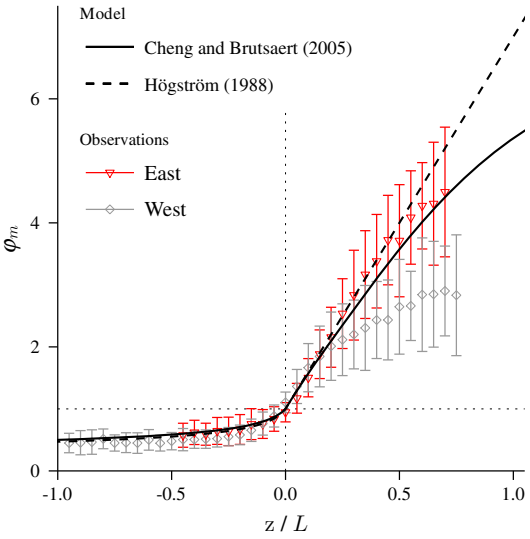

Fig. 9 Dimensionless wind shear ϕ_m as a function of dimensionless stability z/L for the east and west sectors. The data shown have a recovery rate of ≈75 %. The *error bars* denote ±one standard deviation within a z/L bin. Only bins with more than 20 data points are shown

relations from Högström (1988) and the results from Cheng and Brutsaert (2005), who included data from the CASES-99 field experiment. For westerlies and stable conditions ϕ_m is lower than the proposed form of Cheng and Brutsaert (2005) because the surface layer is shallow for westerlies and MOST assumptions are not fulfilled. For easterlies, the form of Cheng and Brutsaert (2005) agrees well with the observations. Analysis of the degree of self-correlation between ϕ_m and z/L for easterlies and $0 < z/L < 1$, using the approach of Mahrt et al. (2003), results in a linear correlation coefficient of 0.91 for the observations and an average value of 0.64 for 1000 trials of randomly-selected data from the observations. This indicates that, although the analysis is not dominated by self-correlation, it is not insignificant at Høvsøre. The degree of self-correlation at Høvsøre is comparable to that estimated using data from the CASES-99 field experiment (Klipp and Mahrt 2004).

6.2 Planetary Boundary Layer

6.2.1 Boundary-Layer Winds

Gryning et al. (2007) proposed a wind-profile model wherein the length scale comprises the inverse summation of the length scales in a three-layer model of the PBL. This model agreed well with the easterly flow observed on the Høvsøre mast and south lighting tower up to 160 m and is dependent on the PBL height. This was estimated by fitting parametrizations of momentum-flux and heat-flux profiles to the observations. Peña et al. (2010c) studied a number of mixing-length models for the neutral PBL and compared the wind-profile expressions derived from the mixing-length models with combined mast-lidar observations of the wind speed up to 300 m and the estimations of the local length scale, $l = u_* (\partial U/\partial z)^{-1}$, with the mixing-length models. The agreement was good for most mixing-length models except for the surface-layer model, which overestimates and underrestimates the observed length scale and wind speed, respectively.

Peña et al. (2010a) extended such mixing-length models to account for stability, and the resulting wind-profile models agreed well with easterly flow-driven wind speeds up to 300 m (from combined mast-lidar measurements). They also showed that the PBL height

can be estimated by averaging vertical profiles of the aerosol backscatter coefficient from a ceilometer under unstable or near-neutral conditions. Other methods for PBL height detection, based on vertical profiles of the vertical velocity variance, were tested on the basis of lidar measurements up to 2000 m (Gürpinar 2011); the profiles showed similar shapes to those from the velocity variance parametrizations in Stull (1988). Peña et al. (2013) investigated several lidar-type instruments and methodologies for PBL height detection, and included a comparison with simulated PBL heights from a numerical weather prediction (NWP) model. In general, they did not find a clear PBL height diurnal variation for easterly flow and the PBL height showed higher values in autumn than in spring. On the basis of the latter work, Hannesdóttir (2013) developed an automated PBL detection algorithm for the ceilometer at Høvsøre.

As horizontal temperature gradients also influence atmospheric flow, Floors et al. (2014) investigated the effect of baroclinity on the vertical wind shear and veer at Høvsøre by analyzing large-scale winds derived from NWP model simulations and lidar wind-speed and direction observations up to 1000 m. They found that the largest thermal wind-velocity vectors at a height of 966 m point northwards and southwards in July and December, respectively, i.e. perpendicular to the sea-land temperature contrast at Høvsøre. They also found that the mean along-wind and transverse wind-speed components deviated from the simulated mean geostrophic components close to the PBL height but approached the geostrophic wind when considering baroclinity. On the basis of these findings the 'Høvsøre tall wind profile' cases were prepared and cover a range of stability, forcing and baroclinic conditions, which can be used to evaluate PBL models (Peña et al. 2014a). Peña et al. (2014b) used several of these cases to study the turning of the wind with height, and found that within the PBL and under barotropic conditions, the more stable the conditions the greater the wind at Høvsøre veered; under baroclinic conditions the wind could even turn anticlockwise.

6.2.2 Internal Boundary Layer

Under westerly flow, the atmosphere at Høvsøre is influenced by the sea-to-land change in roughness conditions and an IBL grows downwind from the coastline. Three types of IBLs can be distinguished: a layer where turbulence is in transition from upwind to downwind conditions (h_i), one where the mean wind is in transition (h_1), and one where the wind is in equilibrium with the downwind surface conditions (h_2), being $h_i > h_1 > h_2$.

A common approach for estimating h_i is based on a diffusion analogy (Miyake 1965). However, when the IBL height is defined by a kink in the wind profile, the upstream logarithmic profile is valid above h_1. From h_2 to h_1, linear interpolation can be used between the upstream and downstream logarithmic wind profiles. Below a height h_2, the wind profile is in equilibrium with the new roughness.

In Floors et al. (2011) the model based on a diffusion analogy was evaluated with the measurements from the Høvsøre mast. When the logarithmic interpolation method by Troen and Petersen (1989) was used, $h_i \approx 220$ m, $h_2 \approx 0.07h_i$ and $h_1 \approx 0.35h_i$. Both upstream and downstream stabilities have a large impact on the wind profile in the IBL, but in the long-term, and in near-neutral conditions, $h_1 \approx$80 m.

6.2.3 Low-Level Jet (LLJ)

The nocturnal LLJ often observed at Høvsøre is of interest for wind-energy purposes because these are associated with high vertical wind shear and increased wind turning over the rotor

area, thereby increasing turbine loading. The climatology of LLJs at Høvsøre was studied using combined lidar/mast wind profiles, applying the same criteria as Baas et al. (2009) and Floors et al. (2013). LLJs occur frequently for southeasterly and northerly flows. Easterlies are favourable for LLJs because during clear nights, jets can form via Coriolis-induced wind oscillations around the geostrophic wind vector (Blackadar 1957). Compared with the climatology of LLJs observed at the Cabauw tower in the Netherlands (Baas et al. 2009), LLJs at Høvsøre seem to be less dependent on the diurnal cycle because of the predominant westerlies (the sea prevents radiative cooling). The jet's maximum speed is Weibull-distributed and is often $\approx$12 m s^{-1}. LLJs typically occur at heights of 100–400 m.

Baroclinity has been found to play a significant role in the LLJ formation at Høvsøre; a decrease of the geostrophic wind speed with height causes a wind-speed maximum at low levels (Peña et al. 2014a; Floors et al. 2014). For a one-year lidar campaign, the easterly flow was on average highly baroclinic (due to a large temperature contrast between land and sea) with a geostrophic wind shear of -3 m s^{-1} km^{-1} and a jet at 600 m. WRF model simulations, made with two different PBL schemes at two different vertical resolutions, tended to underestimate the LLJ magnitude at Høvsøre compared with lidar observations up to 650 m for a four-week period in autumn 2010 (Floors et al. 2013). The LLJ's peak wind speed during a spring night was also underestimated by the WRF model ($\approx$4 m s^{-1} at the simulated PBL height); this LLJ was highly ageostrophic ($\approx$5 m s^{-1} higher than the geostrophic wind). These findings corroborate the results from the GABLS3 intercomparison study (Bosveld et al. 2014) based on measurements from the Cabauw tower.

6.3 Atmospheric Turbulence

The study of atmospheric turbulence is important in wind energy because turbulence is responsible of fatigue damage and affects the power production of turbines. Turbulent fields are used as inputs to aeroelastic load simulations of turbines. Therefore, the Høvsøre dataset provides a basis for studies on turbulence, which have concentrated on microscale turbulence and focused on understanding the turbulence length scales, spectra and fluxes by using both traditional anemometry and lidars.

6.3.1 Traditional Anemometry-Based Studies

Frandsen et al. (2008) deduced turbulence length scales by fitting the empirical spectra of Kaimal et al. (1972) to measurements obtained from the 10-Hz cup anemometer data. They demonstrated that the model in the IEC standards (IEC 2005a) overestimates the turbulence length scales at hub height. This result has an influence on the gust factor and hence the loading of the turbines.

Part of the work has been dedicated to estimating the parameters of the turbulence model developed by Mann (1994). Peña et al. (2010c) for example, derived these parameters by fitting the one-dimensional turbulence spectra from the sonic measurements at different heights to the Mann model under near-neutral conditions and found a direct relation between the turbulence and the mixing-length scales. Later, Peña et al. (2010b) derived the same parameters under different atmospheric stability conditions and found similar relations between length scales. These results demonstrate the close connection between the wind profile and the turbulence structure.

Sathe et al. (2013) re-derived the Mann model parameters to estimate the impact of turbulence under different stabilities on turbine loads. By including stability effects, they found that the loads on a number of turbine components increased up to 17% compared to the neutral

case. Chougule et al. (2012) performed a study of the cross-spectral phases between different wind-field components at two heights at Høvsøre using the Mann model parameters and sonic measurements. Such a study provides insights into, e.g. the influence of shear-induced turbulence on the turbine rotor. A comparison of the derived Mann model parameters between agricultural (Høvsøre) and forested landscapes was conducted by Chougule et al. (2015), where significant differences in the dissipation rate parameter were observed. In addition, Chougule (2013) developed a stability-dependent spectral tensor model, which builds on the neutral Mann model, and found good agreement between the model results and measurements at the Høvsøre mast.

6.3.2 Lidar-Based Studies

Sjöholm et al. (2009) modelled the spatial averaging effect within the probe volume of a continuous wave lidar and evaluated the model with Høvsøre measurements. Later, Mann et al. (2009) modelled the same effects for a pulsed lidar. Both studies demonstrated that only large-scale turbulence could be measured due to the lidar's probe volume averaging effect and used the Mann model to prove the lidar turbulence 'filtering' phenomenon.

Mann et al. (2010) discussed the measurement of momentum flux with scanning lidars; depending on the height and the lidar type, the flux was underestimated ≈69–93 %. In the latter study, a model compensating for the spatial averaging effect was also developed enabling the measurement of the unfiltered momentum flux. Model evaluation was performed using sonic measurements, and the scatter plots showed linear regressions in the range of 1.00 to 1.07. Berg et al. (2011) measured the stress vectors and the vertical gradient of the mean velocity vector using lidars and sonics and found significant deviations between the two vectors even at 100 m. Sathe et al. (2011) modelled the lidar turbulence for all components of the Reynolds stress tensor using the velocity azimuth display (VAD) method. Here, two effects causing incorrect estimations of turbulence with lidars were identified: (1) spatial averaging, and (2) cross-contamination by the different wind-field components. The two effects compensate each other and thus 'accurate' turbulence measurements can be found for the wrong reasons. The addition/filtering of turbulence depends on the type of lidar, the turbulence structure, and the measurement height. They compared sonic measurements at several heights on the Høvsøre mast with VAD lidars' measurements, where up to 90 and 70 % of turbulence filtering was observed for the vertical and horizontal velocity variances.

Sathe and Mann (2012) investigated measured turbulence spectra from a scanning pulsed lidar using VAD data analysis, where the spatial averaging and cross-contamination effects were evident within the inertial sub-range. The above studies have pushed the use of either multiple lidars staring at a point or methodologies using a single lidar to measure turbulence. Sathe (2012) used a six-beam method to estimate turbulence statistics from the radial velocity variances rather than the radial velocity measurements. The cross-contamination effect is minimized using this method, but compensating for the spatial averaging effects for pulsed lidars still remains a challenge. Experimental evidence suggests that the six-beam method partly overcomes the problem of probe volume averaging that is inherent in the VAD method (Sathe et al. 2015).

6.4 Numerical Modelling

Numerical modelling has been performed for flow at the Høvsøre site for several years, particularly for evaluating mesoscale models. Microscale flow models have been used and evaluated for applied use in wind-power meteorology (Sect. 4.2) and IBL studies (Sect. 6.2.2).

6.4.1 Numerical Weather Prediction

The first mesoscale-type studies of the Høvsøre wind climate were performed by Nissen (2008). He studied the seasonal evolution of the wind field to improve the understanding of the role of the marine boundary layer on coastal winds. The study used mesoscale model simulations from the USA Naval Research Laboratory COAMPS model (Chen et al. 2003). Westerlies showed increased wind variability during spring and winter compared with that during summer and autumn (Nissen and Gryning 2010). The excess temperature over England relative to that over the North Sea was shown to trigger boundary-layer oscillations, usually in the form of gravity waves, which could explain the increased observed wind variance.

Later, WRF model simulations covering the Høvsøre area became frequent as these are used to derive wind atlases by combining both mesoscale and microscale models (e.g. see http://www.wasaproject.info). Wind speeds, temperatures and vertical wind shears simulated by the model were evaluated against Høvsøre measurements by Draxl et al. (2014). Different PBL schemes were examined to determine which parametrization performs best for wind-energy forecasting. The results showed that the performance of the simulations was highly dependent on stability; simulations tended to show vertical wind shear less than that observed in agreement with Floors et al. (2013). Similar evaluations using Høvsøre measurements were performed in Hahmann et al. (2012). These model deficiencies are not unique to Høvsøre and have also been identified at other sites (Storm and Basu 2010; Kleczek et al. 2014).

Temperature measurements from the Høvsøre mast were used to evaluate the accuracy of nacelle temperature measurements. The results proved to be highly sensitive to the location of the temperature sensor on the turbine. Mast and nacelle temperature measurements were compared to WRF model simulations. The WRF model was found to have a cold bias of $-0.6\,^{\circ}\mathrm{C}$ at 100 m compared with the mast measurements (Davis 2014). The errors in the nacelle-measured and WRF model-simulated temperatures have implications for identifying winds under icing events on turbines, which are important, for example, for the determination of the turbine' power curve and for the control of the machine.

Using the WRF model, a 6-year mesoscale reanalysis simulation was conducted for the North and Baltic Seas (Hahmann et al. 2015). The results of the simulation were verified against various offshore and coastal sites including Høvsøre. At 100 m, the winds simulated by the WRF model underestimated the observed long-term average wind speed by -1.3 %. The measurements were also used to demonstrate the lack of sensitivity of the simulated long-term mean wind speed (offshore in this case) on many aspects of the model set-up, including the type of reanalysis used, resolution of sea-surface temperatures, number of vertical levels, and strength and form of the nudging. The impact of nudging on the simulated wind profile of the WRF model up to 600 m at Høvsøre was investigated by Gryning et al. (2013) using a 1-year period of lidar-mast measurements. A minor impact on the simulated mean values was found and an underestimation of the mean wind speed, turning of the wind and wind power-density profiles by the WRF model revealed. Nudging was found to reduce the scatter between the simulated and measured wind speeds.

Other NWP outputs over the Høvsøre area were used to estimate the geostrophic, thermal and gradient winds. These 'large-scale' winds provided further understanding of the observed vertical wind shear and wind turning at Høvsøre for a 1-yr lidar campaign; particularly close to the PBL height, baroclinity was found to significantly influence the wind at Høvsøre (Peña et al. 2014a; Floors et al. 2014).

Floors et al. (2013) used two roughness descriptions to simulate the flow at Høvsøre with the WRF model: the standard one based on MODIS land-cover data[2] and the other based on observations at Høvsøre (z_o was computed similarly as shown in Sect. 3). Using the standard description, they found an ≈10 % lower mean wind speed at 10 m when compared with that using a more realistic surface roughness description for westerlies. However, little effect was noticed at 100-m for westerlies. When using mesoscale models, it is very important to understand the resolution dependency on the flow response of the strong roughness changes; simulated winds by the WRF model take nearly the same number of grid points to adjust to the new surface conditions regardless of the grid spacing (Vincent et al. 2013).

6.4.2 Large-Eddy Simulation

Pedersen et al. (2013) studied the ability of large-eddy simulation to model the PBL at Høvsøre. They included temporal and spatial variations of the external forcing applied as a pressure gradient across the domain. During one day in May and for easterly flow, lidar measurements showed a general increase in wind speed during the day, and a decrease with height above the PBL height (an indication of baroclinic conditions and of a decreasing driving large-scale pressure gradient with height). The observations were compared with many simulations wherein the variations in the large-scale pressure field were imposed in the model boundary conditions through progressively more realistic forcing. They found that including both height and time variations in the applied pressure gradient improved the agreement with the observations.

6.5 Offshore Wind

The observations at Høvsøre have been used for offshore wind resource assessment. Research using satellite Synthetic Aperture Radar (SAR) data reported accuracy similar to the mesoscale modelling when compared with wind speed observations (Badger et al. 2010). The Høvsøre data were analyzed using WAsP at a location a few kilometres offshore where satellite SAR data are available.

7 Perspectives and Lessons Learned

The Høvsøre site has provided wind-power and boundary-layer scientists and specialists with a high-quality, long-term, complete dataset of meteorological data for more than 10 years and it has been the basis for multidisciplinary studies and research campaigns. However, Høvsøre is far from being fully exploited. There have been few attempts to evaluate microscale models able to simulate the wind-speed diurnal cycle; this is surprising since these are the same models used for wind resource assessment and turbine siting.

Reanalysis products per se have not been evaluated at Høvsøre, which is not only important for optimizing the outcome of numerical simulations for the region, but also to evaluate the wind and climate variability studies themselves. This is very valuable for countries such as Denmark, where wind energy accounted for ≈39 % of the country's electricity consumption in 2014. Wind-energy performance indicators, such as the wind-power production index for Denmark, which show inter- and intra-annual variations, could potentially be compared with

[2] http://daac.ornl.gov/MODIS/MODIS-menu/MCD12Q1_known_issues.html.

the Høvsøre dataset. In addition, Høvsøre provides a rich dataset for studies on the sea-land transition and coastal effects, which are notoriously difficult to model with NWP models.

The database contains 'fast' raw data from the sonic anemometers, which provide the basis for research on gusts; nevertheless, the topic has received limited attention. For westerly flow, the effect of the sea-land transition on the Weibull shape parameter peak height is not well understood but preliminary analysis shows that this behaves similarly to the IBL at Høvsøre.

Acknowledgments Funding from the Danish Council for Strategic Research Project no. 2104-08-0025 'Tall Wind' project and the Danish Ministry of Science, Innovation and Higher Education—Technology and Production, grant no. 0602-02486B are acknowledged. This work was inspired by the review paper on atmospheric boundary layer research at Cabauw by van Ulden and Wieringa (1996) and was conducted by collaboration between the Test and Measurements and the Meteorology sections at the Wind Energy Department of the Technical University of Denmark. We would also like to thank Peter Hjuler Jensen for recalling the history of Høvsøre and the anonymous reviewers for their valuable comments.

References

Albers A, Franke K, Wagner R, Courtney M, Boquet M (2012) 'Ground-based remote sensor uncertainty - a case study for a wind lidar'. In: Proc. EWEA. Copenhagen

Baas P, Bosveld FC, Baltink HK, Holtslag AAM (2009) A climatology of nocturnal low-level jets at Cabauw. J Appl Meteorol Clim 48:1627–1642

Badger M, Badger J, Nielsen M, Hasager CB, Peña A (2010) Wind class sampling of satellite SAR imagery for offshore wind resource mapping. J Appl Meteorol Clim 49:2474–2491

Berg J, Mann J, Patton E (2011) Lidar-observed stress vectors and veer in the atmospheric boundary layer. J Atmos Ocean Technol 30:1961–1969

Blackadar AK (1957) Boundary layer wind maxima and their significance for the growth of nocturnal inversions. Bull Am Meteorol Soc 38:283–290

Blatt A (2010) Roughness length analysis for wind energy purposes. Technical Report Master Thesis, Risø DTU, Roskilde, 114 pp

Bosveld FC, Baas P, Steeneveld G-J, Holtslag AAM, Angevine WM, Bazile E, de Bruijn EIF, Deacu D, Edwards JM, Ek M, Larson VE, Pleim JE, Raschendorfer M, Svensson G (2014) The third GABLS intercomparison case for evaluation studies of boundary-layer models. Part B: results and process understanding. Bound-Layer Meteorol 152:157–187

Bradley SG, Antoniou I, Hunerbein SV, Kindler D, Jørgensen HE, Noord MD (2005) SODAR calibration for wind energy applications, final reporting on WP3, EU WISE project NN5-2001-297. Technical Report University of Salford, Salford, 68 pp

Brasseur O (2001) Development and application of a physical approach to estimating wind gusts. Mon Weather Rev 129:5–25

Chen S, Cummings J, Doyle J, Hodur R, Holtt T, Liou CS, Liu M, Ridout J, Schmidt J, Thompson W, Mirin A, Sugiyama G (2003) 'COAMPS version 3 model description - general theory and equations'. Technical Report NRL/PU/7500-04-448, Naval Research Laboratory, Marine Meteorology Division, Monterey

Cheng Y, Brutsaert W (2005) Flux-profile relationships for wind speed and temperature in the stable atmospheric boundary layer. Boundary-Layer Meteorol 114:519–538

Chougule A (2013) 'Influence of atmospheric stability on the spatial structure of turbulence'. Technical Report PhD-028(EN), DTU Wind Energy, Roskilde, 97 pp

Chougule A, Mann J, Kelly M, Sun J, Lenschow DH, Patton EG (2012) Vertical cross-spectral phases in neutral atmospheric flow. J Turbul 13(36):1–13

Chougule A, Mann J, Segalini A, Dellwik E (2015) Spectral tensor parameters for wind turbine load modeling from forested and agricultural landscapes. Wind Energy 18:469–481

Courtney M, Peña A, Wagner R, Peeringa J, Brand A, Gottschall J, Rettenmeier A, Pierella F (2014) D4.06 Data reports and databases: Data on coastal and offshore wind measurements. Technical report, Marine Renewables Infrastructure Network (MARINET), Roskilde, 42 pp

Davis N (2014) Icing impacts on wind energy production. Technical Report PhD-0025(EN), DTU Wind Energy, Roskilde, 126 pp
Dellwik E, Mann J, Bingöl F (2010) Flow tilt angles near forest edges–Part 2: Lidar anemometry. Biogeo 7:1759–1768
DMEE (2000) National prøvestation for store vindmøller: vuerdering af virkningen på miljøet (VVM): redegørelse. Technical report, Danish Ministry of Environment and Energy and Risø National Laboratory, Copenhagen, 192 pp
Draxl C, Hahmann AN, Peña A, Giebel G (2014) Evaluating winds and vertical wind shear from Weather Research and Forecasting model forecasts using seven planetary boundary layer schemes. Wind Energy 17:39–55
Dyer AJ (1974) A review of flux-profile relationships. Boundary-Layer Meteorol 7:363–372
Floors R, Gryning S-E, Peña A, Batchvarova E (2011) Analysis of diabatic flow modification in the internal boundary layer. Meteorol Z 20:649–659
Floors R, Peña A, Gryning S-E (2014) Gryning S-E (2014) The effect of baroclinity on the wind in the planetary boundary layer. Q J R Meteorol Soc 141:619–630
Floors R, Vincent CL, Gryning S-E, Peña A, Batchvarova E (2013) The wind profile in the coastal boundary layer: wind lidar measurements and numerical modelling. Boundary-Layer Meteorol 147:469–491
Frandsen S, Jørgensen HE, Sørensen JD (2008) Relevant criteria for testing the quality of models for turbulent wind speed fluctuations. J Solar Energy T ASME 130:031016, 7 pp
Gürpinar MA (2011) Estimating atmospheric boundary layer height from vertical sigma w profiles and parameterization of vertical variances - by LIDARS at Høvsøre (Denmark). Technical Report EGI-2011-111MSC/EKV:859, KTH School of Industrial Engineering and Management, Stockholm, 85 pp
Gryning S-E, Batchvarova E, Brümmer B, Jørgensen H, Larsen S (2007) On the extension of the wind profile over homogeneous terrain beyond the surface layer. Boundary-Layer Meteorol 124:251–268
Gryning S-E, Batchvarova E, Floors R (2013) A study on the effect of nudging on long-term boundary-layer profiles of wind and Weibull distribution parameters in a rural coastal area. J Appl Meteorol Clim 52:1201–1207
Gryning S-E, Batchvarova E, Floors R, Peña A, Brümmer B, Hahmann AN, Mikkelsen T (2014) Long-term profiles of wind and Weibull distribution parameters up to 600 m in a rural coastal and an inland suburban area. Boundary-Layer Meteorol 150:167–184
Hahmann AN, Lange J, Peña A, Hasager CB (2012) 'The NORSEWInD numerical wind atlas for the South Baltic'. Technical Report E-Report-0011(EN), DTU Wind Energy, Roskilde, 52 pp
Hahmann AN, Vincent C, Peña A, Lange J, Hasager CB (2015) 'Wind climate estimation using WRF model output: Method and model sensitivities over the sea'. Int. J. Climatol. doi:10.1002/joc.4217
Hannesdóttir A (2013) 'Boundary-layer height detection with a ceilometer at a coastal site in western Denmark'. Technical Report Master Thesis M-0039, DTU Wind Energy, Roskilde, 76 pp
Hasager CB, Stein D, Courtney M, Peña A, Mikkelsen T, Stickland M, Oldroyd A (2013) Hub height ocean winds over the North Sea observed by the NORSEWInD lidar array: measurement techniques, quality control and data management. Remote Sens 5:4280–4303
Högström U (1988) Non-dimensional wind and temperature profiles in the atmospheric surface layer: a re-evaluation. Boundary-Layer Meteorol 42:55–78
IEC (2005a) IEC 61400–1. Wind turbines–Part 1: design requirements. International standard,International Electrotechnical Commission, Geneva, 92 pp
IEC (2005b) IEC 61400–12-1. Wind turbines–Part 12–1: power performance measurements of electricity producing wind turbines. International standard,International Electrotechnical Commission, Geneva, 90 pp
Kaimal JC, Wyngaard JC, Izumi Y, Cote OR (1972) Spectral characteristics of surface-layer turbulence. Q J R Meteorol Soc 98:563–589
Kelly M, Gryning S-E (2010) Long-term wind profiles based on similarity theory. Boundary-Layer Meteorol 136:377–390
Kelly M, Troen I, Jørgensen HE (2014) Weibull-*k* revisited: "Tall" profiles and height variation of wind statistics. Boundary-Layer Meteorol 152:107–124
Kleczek MA, Steeneveld G-J, Holtslag AAM (2014) Evaluation of the Weather Research and Forecasting mesoscale model for GABLS3: impact of boundary-layer schemes, boundary conditions and spin-up. Boundary-Layer Meteorol 152:213–243
Klipp CL, Mahrt L (2004) Flux-gradient relationship, self-correlation and intermittency in the stable boundary layer. Q J R Meteorol Soc 130:2087–2103
Larsén XG, Kruger A (2014) 'Extreme gust estimation using mesoscale modeling'. In: Proc. of EWEA. Barcelona

Larsén XG, Ott S, Badger J, Hahmann AN, Mann J (2012) Recepies for correcting the impact of effective mesoscale resolution on the estimation of extreme winds. J Appl Meteorol Clim 51:521–533
Larsén XG, Badger J, Hahmann AN, Mortensen NG (2013a) The selective dynamical downscaling method for extreme-wind atlases. Wind Energy 16:1167–1182
Larsén XG, Vincent CL, Larsen S (2013b) Spectral structure of the mesoscale winds over the water. Q J R Meteorol Soc 139:685–700
Lindelöw-Marsden P (2007) 'UpWind D1. Uncertainties in wind assessment with LIDAR'. Technical Report Risø-R-1681(EN), Risø DTU, Roskilde, 54 pp
Mahrt L, Vickers D, Frederickson P, Davidson K, Smedman A-S (2003) Sea-surface aerodynamic roughness. J Geophys Res 108(C6):3171
Mann J (1994) The spatial structure of neutral atmospheric surface-layer turbulence. J Fluid Mech 273:141–168
Mann J, Cariou J-P, Courtney MS, Parmentier R, Mikkelsen T, Wagner R, Lindelöw P, Sjöholm M, Enevoldsen K (2009) Comparison of 3D turbulence measurements using three staring wind lidars and a sonic anemometer. Meteorol Z 18:135–140
Mann J, Peña A, Bingöl F, Wagner R, Courtney MS (2010) Lidar scanning of momentum flux in and above the surface layer. J Atmos Ocean Tech 27:959–976
Miyake M (1965) Transformation of the atmospheric boundary layer over inhomogeneous surfaces. Technical Report Unpublished MSc. Thesis, Sci. Rep. 5R–6, University of Washington, Seattle, 63 pp
Mortensen NG, Heathfield DN, Myllerup L, Landberg L, Rathmann O (2007) Getting started with WAsP 9. Technical Report Risø-I-2571(EN), Risø National Laboratory
Nissen JN (2008) 'On the application of a numerical model to simulate the coastal boundary layer'. PhD-thesis Risø-PhD-39(EN), Risø National Laboratory, Roskilde, 110 pp
Nissen JN, Gryning S-E (2010) Seasonality in onshore normalized wind profiles above the surface layer. Adv Sci Res 4:57–62
Obukhov AM (1971) Turbulence in an atmosphere with a non-uniform temperature. Boundary-Layer Meteorol 2:7–29
Peña A (2009) 'Sensing the wind profile'. Technical Report Risø-PhD-45(EN), Risø DTU, Roskilde, 88 pp
Peña A, Gryning S-E, Hasager CB (2010a) Comparing mixing-length models of the diabatic wind profile over homogeneous terrain. Theor Appl Clim 100:325–335
Peña A, Gryning S-E, Mann J (2010b) On the length scale of the wind profile. Q J R Meteorol Soc 136:2119–2131
Peña A, Gryning S-E, Mann J, Hasager CB (2010c) Length scales of the neutral wind profile over homogeneous terrain. J Appl Meteorol Clim 49:792–806
Peña A, Mikkelsen T, Gryning S-E, Hasager CB, Hahmann A, Badger M, Karagali I, Courtney M (2012) Offshore vertical wind shear: Final report on NORSEWInD's work task 3.1, E-Report-0005(EN). DTU Wind Energy, Roskilde, 112 pp
Peña A, Gryning S-E, Hahmann AN (2013) Observations of the atmospheric boundary layer height under marine upstream flow conditions at a coastal site. J Geophys Res Atmos 118:1924–1940
Peña A, Floors R, Gryning S-E (2014a) The Høvsøre tall wind-profile experiment: a description of wind profile observations in the atmospheric boundary layer. Boundary-Layer Meteorol 150:69–89
Peña A, Gryning S-E, Floors R (2014b) The turning of the wind in the atmospheric boundary layer. J Phys Conf Ser 524: 012118, 8 pp
Peña A, Réthoré P-E, van der Laan MP (2015a) 'On the application of the Jensen wake model using a turbulence-dependent wake decay coefficient: The Sexbierum case'. Wind Energy. doi:10.1002/we.1863
Peña A, Floors R, Gryning S-E (2015b) Reply to the comment by Bergmann on "The Høvsøre tall wind-profile experiment: a description of wind profile observations in the atmospheric boundary layer". Boundary-Layer Meteorol. doi:10.1007/s10546-015-0077-x
Pedersen JG, Kelly M, Gryning S-E, Brümmer B (2013) The effect of unsteady and baroclinic forcing on predicted wind profiles in Large Eddy Simulations: Two case studies of the daytime atmospheric boundary layer. Meteorol Z 22:661–674
Perez-Andujar A (2013) 'Long-term corrections for wind resource assessment'. Technical Report Master-Series-M-0047(EN), DTU Wind Energy, Roskilde, 100 pp
Petersen EL, Mortensen NG, Landberg L, Højstrup J, Frank HP (1998) Wind power meteorology. Part I: Climate and turbulence. Wind Energy 1:25–45
Sathe A (2012) 'Influence of wind conditions on wind turbine loads and measurement of turbulence using lidars'. PhD Thesis, Delft University of Technology, Delft, 139 pp
Sathe A, Mann J (2012) 'Measurement of turbulence spectra using scanning pulsed wind lidars'. J. Geophys. Res. 117:D01201 (11 pp)
Sathe A, Mann J, Gottschall J, Courtney MS (2011) Can wind lidars measure turbulence? J Atmos Ocean Technol 28:853–868

Sathe A, Mann J, Barlas T, Bierbooms WAAM, van Bussel GJW (2013) Influence of atmospheric stability on wind turbine loads. Wind Energy 16:1013–1032

Sathe A, Mann J, Vasiljevic N, Lea G (2015) A six-beam method to measure turbulence statistics using ground-based wind lidars. Atmos Meas Tech 8:729–740

Sjöholm M, Mikkelsen T, Mann J, Enevoldsen K, Courtney M (2009) Spatial averaging-effects on turbulence measured by a continuous-wave coherent lidar. Meteorol Z 18:281–287

Skamarock WC (2004) Evaluating mesoscale NWP models using kinetic energy spectra. Mon Weather Rev 132:3019–3032

Skamarock WC, Klemp JB, Dudhia J, Gill DO, Barker DM, Duda MG, Huang X-Y, Wang W, Powers JG (2008) A description of the advanced research WRF version 3. Technical Report NCAR/TN-475+STR, Mesoscale and Microscale Meteorology Division, National Center for Atmospheric Research, Boulder, Colorado, USA

Storm B, Basu S (2010) The WRF model forecast-derived low-level wind shear climatology over the United States Great Plains. Energies 3:258–276

Stull RB (1988) An introduction to boundary layer meteorology. Kluwer Academic Publishers, Dordrecht, 666 pp

Suomi I, Gryning S-E, Floors R, Vihma T, Fortelius C (2014) On the vertical structure of wind gusts. Q J R Meteorol Soc 141:1658–1670

TPWind (2014) Strategic Research Agenda/Market Deployment Strategy (SRA/MDS). Technical report, European Wind Energy Technology Platform, Brussels 79 pp

Troen I, Petersen EL (1989) European Wind Atlas. Risø National Laboratory, Roskilde 656 pp

van Ulden AP, Wieringa J (1996) Atmospheric boundary layer research at Cabauw. Boundary-Layer Meteorol 78:39–69

Vincent CL, Badger J, Hahmann AN, Kelly MC (2013) The response of mesoscale models to changes in surface roughness. In: Geophysical Research Abstracts, vol 13, pp EGU2013-8548

Wagner R, Antoniou I, Pedersen SM, Courtney M, Courtney M, Jørgensen HE (2009) The influence of the wind speed profile on wind turbine performance measurements. Wind Energy 12:348–362

Wagner R, Courtney M, Gottschall J, Lindelöw-Marsden P (2011) Accounting of the speed shear in wind turbine power performance measurement. Wind Energy 14:993–1004

Wagner R, Rivera RL, Antoniou I, Davoust S, Pedersen TF, Courtney M, Diznabi B (2013) Procedure for wind turbine power performance measurement with a two-beam nacelle lidar. Technical Report. DTU Wind Energy-E-0019, DTU Wind Energy, Roskilde, 28 pp

Wagner R, Pedersen TF, Courtney M, Antoniou I, Davoust S, Rivera RL (2014b) Power curve measurement with a nacelle mounted lidar. Wind Energy 17:1441–1453